Coarse graining the Bethe–Goldstone equation: Nucleon–nucleon high-momentum components

I. Ruiz Simo,[1,*] R. Navarro Pérez,[2,†] J. E. Amaro,[1,‡] and E. Ruiz Arriola[1,§]

[1]*Department of Atomic, Molecular, and Nuclear Physics and Carlos I Institute of Theoretical and Computational Physics, University of Granada, E-18071 Granada, Spain*

[2]*Nuclear and Chemical Sciences Division, Lawrence Livermore National Laboratory, Livermore, CA 94551, USA*

(Received 4 August 2017; published 27 November 2017)

The δ-shell representation of the nuclear force allows a simplified treatment of nuclear correlations. We show how this applies to the Bethe–Goldstone equation as an integral equation in coordinate space with a few mesh points, which is solved by inversion of a five-dimensional square matrix in the single channel cases and a 10×10 matrix for the tensor-coupled channels. This allows us to readily obtain the high-momentum distribution, for all partial waves, of a back-to-back correlated nucleon pair in nuclear matter. We find that the probability of finding a high-momentum correlated neutron–proton pair is about 18 times that of a proton–proton one, as a result of the strong tensor force, thus confirming in an independent way previous results and measurements.

DOI: 10.1103/PhysRevC.96.054006

I. INTRODUCTION

Nuclear correlations have been a topic of discussion in nuclear matter and finite nuclei calculations for a long time. The starting point is the fundamental nucleon–nucleon (NN) interaction, which has been determined from the available NN-scattering data. Most local interactions which have been proposed so far retain in common a short-distance repulsion, a feature discovered by Jastrow in 1950 when he analyzed proton–proton (pp) scattering at intermediate laboratory (Lab.) energies [1,2]. Its main natural consequence is the presence of short-distance correlations, which invalidates perturbation theory based on a mean-field approach. There have been proposed many ways to conveniently address these short-distance features. Historically the Bethe–Goldstone (BG) equation [3] was the first proposal with consequences for the nuclear wave functions [4,5] (see, e.g., Ref. [6] for a modern review).

When two nucleons in a nuclear medium approach each other the relative wave function is less sensitive to the particular long-range details of the nucleus where they are embedded. Hence one expects the medium effects at short distances to be mainly driven on average by the Pauli principle, forbidding the two nucleons to scatter below some typical Fermi momentum. The effect of the interaction will produce a slight but rapid—high-momentum—vibration in the relative wave function at short distances. This distortion of the unperturbed wave function at mid- and short ranges induces naturally an universal behavior at high momenta [7–9].

From the theoretical point of view, the short-range nucleon–nucleon correlations (SRC) are ubiquitous, appearing in different contexts ranging from fundamental to applied nuclear physics: properties of nuclear matter [10–12], high-momentum components in the nuclear wave function [13–17], nuclear astrophysics [18], calculations of symmetry energy and pairing gaps in nuclear and neutron matter [19–21], equation of state of nuclear matter [22,23], models of relativistic heavy-ion collisions [24], calculations of nuclear matrix elements for neutrino-less double beta decay [25,26], and description of (e,e'), $(e,e'N)$, and $(e,e'NN)$ reactions [27–31], just to highlight some of them.

From the experimental side, the insight into the mass and isospin dependence of SRC is field of active research [32–41]. For example, by measuring the ratio of neutron–proton (np) and proton–proton (pp) pairs in a relative high-momentum state, a value of $np/pp = 18 \pm 5$ was reported in Ref. [32], providing strong evidence of the crucial impact of the tensor force in the SRC. This suggest a nontrivial dependence of SRC on the N–Z asymmetry, with repercussions on the nuclear equation of state for high densities, which is essential for the understanding of neutron stars [42,43].

In order to justify our approach to SRC to be detailed below it is important to remind some relevant features. The standard approach for *ab initio* calculations since the benchmarking analysis of the Nijmegen group has been based on a two-step process. In a first step, a partial wave analysis to NN-scattering data was carried out [44] and a selection of consistent data was implemented on the basis of statistical significance. The Nijmegen NN database had 4313 $pp + np$ selected scattering data for $T_{\rm LAB} \leqslant 350$ MeV improving on previous approaches [45,46] due to the incorporation of small but crucial long-distance effects, such as charge-dependent one-pion-exchange (CD-OPE), vacuum polarization, and Coulomb, relativistic, and magnetic moments interactions. Unfortunately, the energy dependence of the potential is hard to implement in nuclear structure calculations. Therefore, in a second step an energy-independent potential often tailored to a particular solution method of the nuclear many-body problem was constructed and fitted to the database. In this way, a set of high-quality statistically equivalent potentials have been designed [47–50]. This may introduce a bias and hence a source of systematic error in the design of the starting nuclear force, and in particular into its short-distance structure. Thus, it would be desirable that the potential represents as closely as possible the scattering data used for its construction.

*ruizsig@ugr.es
†navarroperez1@llnl.gov
‡amaro@ugr.es
§earriola@ugr.es

In the present work we deepen our investigation into the basic theoretical understanding of SRC by employing the coarse-grained Granada potential (GR) in our analysis. In common with the Nijmegen analysis, this potential contains all long-distance effects such as CD-OPE, Coulomb, vacuum polarization, and relativistic and magnetic moments effects above a separation distance of $r_c = 3$ fm and a sum of equidistant Dirac δ shells below that distance. The complete potential has been used to generate the Granada-2013 database, a 3σ self-consistent selection of 6173-NN-scattering data of the about 8000 collected between 1950 and 2013 at about pion production threshold, $T_{\rm LAB} \leqslant 350$ MeV with a reduced $\chi^2/\nu \sim 1.04$ [51–53]. This representation of the NN interaction is very convenient not only because it samples *directly* the interaction at the physically significant resolution $\Delta r \sim 1/p_{\rm c.m.} \sim 0.6$ fm (where c.m. is center of mass) associated with a maximum fitting momentum $p_{\rm c.m.} \lesssim \sqrt{M_N m_\pi}$ but also because it implies a great simplification of the nuclear problem in terms of few grid points in coordinate space located at δ shells whose strengths correspond to the fitting parameters. This way, we short-circuit the two-step process mentioned above. The bias induced by different representations using different potential tails or short range representations has been illustrated with six different statistically equivalent Granada potentials fitting the same database [54].

Of course, this simplification is not for free, as new computational methods need to be developed to handle this successful but unconventional δ-shell representation of the nuclear force. As a rewarding consequence, it allows a deeper understanding of the role of the short and mid-range part of the NN interaction in the SRC. The present study of the coarse-grained Bethe–Goldstone equation was initiated in our recent work [55] for the $^1S_0$ partial wave. Here we extended it to all the partial waves and analyze the consequences. We study the problem from an integral equation point of view in coordinate space. This approach has clear advantages compared to the integrodifferential formulation of our previous work [55]. In particular, the boundary conditions for the scattering problem in the nuclear medium are automatically incorporated into the integral equation. In addition, we shall show that the implementation of coupled channels is rather straightforward.

In this first exploring work we avoid the problem related with inelasticities, which are expected to become important at relative momenta above the Δ production threshold. The high-quality NN interactions traditionally used to deal with SRC, as is also the case of the coarse-grained potential used in this paper, have been fitted to NN elastic scattering about pion emission. This imposes limits for the maximum value of the high-momentum components and the meaning of the predictions for high-momentum components above 2–3 k_F with a real potential should be taken with care. In a recent paper coarse graining has been shown to work nicely up to scattering LAB energies of 3 GeV [56], in this case including inelasticity effects. However, the analysis of the Bethe–Goldstone equation including inelasticities through a complex potential will be postponed for a future work.

The outline of the paper is as follows: In Sec. II we review the partial-wave (PW) integral equations formalism of the scattering problem before introducing in Sec. III the BG equation in coordinate space. We particularize to the case of a coarse-grained potential with δ shells, where the equations can be discretized and solved by inversion of low-dimension matrices. Next we proceed to momentum space and get the expressions for the high-momentum components of the BG solution for a correlated pair in the PW expansion. In Sec. IV we apply the formalism to the coarse-grained Granada potential, obtained in a recent partial-wave analysis of a large, consistent database of NN-scattering data with $\chi^2/\nu \sim 1$ [51,52]. The BG equation in nuclear matter is solved for the first partial waves up to the $^3F_2$ and the solutions are analyzed both in coordinate and momentum space, which allows us to obtain the high-momentum distribution of np and pp correlated pairs. Finally we draw our conclusions in Sec. V and discuss future applications of this approach.

II. THE INTEGRAL SCATTERING EQUATION

Before introducing the BG equation, it is instructive to review the particular case of the scattering equation in the vacuum in the partial waves representation (see also the Appendices of Ref. [57] for more details). The Schroedinger equation for the reduced relative wave function of a pair of nucleons interacting through a two-body potential can be written for coupled channels (and therefore for total spin $S = 1$),

$$u''_{k,l}(r) - \left[\frac{l(l+1)}{r^2} - k^2\right] u_{k,l}(r) = \sum_{l'} U_{l,l'}(r) u_{k,l'}(r), \quad (1)$$

where l is the orbital angular-momentum quantum number, $U_{l,l'}(r)$, is the, in general, nondiagonal reduced potential and the sum has to be carried out over all partial waves coupled by the interaction.

These equations are subjected to the usual scattering asymptotic boundary conditions and can equivalently be written as a system of integral equations,

$$u_{k,l}(r) = \hat{j}_l(kr) + \int_0^\infty dr'\, G_{k,l}(r,r') \sum_{l'} U_{l,l'}(r')\, u_{k,l'}(r'), \quad (2)$$

where $\hat{j}_l(x) = x j_l(x)$ is a reduced spherical Bessel function of the first kind and $G_{k,l}(r,r')$ is the Green's function satisfying

$$\left\{\frac{\partial^2}{\partial r^2} - \left[\frac{l(l+1)}{r^2} - k^2\right]\right\} G_{k,l}(r,r') = \delta(r - r'). \quad (3)$$

The normalization chosen in Eq. (2) implies that the reduced wave function $u_{k,l}(r)$ is dimensionless. This normalization for the relative wave functions is consistent with that employed in our previous work [55] for the uncoupled $^1S_0$ channel.

An analytic expression for the Green's function $G_{k,l}(r,r')$ can be written as

$$G_{k,l}(r,r') = u(r)v(r')\theta(r - r') + u(r')v(r)\theta(r' - r). \quad (4)$$

Inserting this into Eq. (3), it follows that $u(r)$ and $v(r)$ are solutions of the homogeneous equation with unit Wronskian, i.e.,

$$\left\{\frac{\partial^2}{\partial r^2}-\left[\frac{l(l+1)}{r^2}-k^2\right]\right\}u(r)=0, \tag{5}$$

$$\left\{\frac{\partial^2}{\partial r^2}-\left[\frac{l(l+1)}{r^2}-k^2\right]\right\}v(r)=0, \tag{6}$$

$$u'(r)v(r)-u(r)v'(r)=1. \tag{7}$$

We choose one of the two solutions to be proportional to the regular solution, $\hat{j}_l(kr)$. Then the other linearly independent solution with the desired Wronskian has to be proportional to $\hat{y}_l(kr)=kr\ y_l(kr)$—the reduced spherical Bessel function of the second kind. Therefore the Green's function of the ordinary differential equation with the proper normalization can be written as

$$G_{k,l}(r,r')=\frac{1}{k}\,\hat{j}_l(kr_<)\,\hat{y}_l(kr_>), \tag{8}$$

where $r_<=\min\{r,r'\}$ and $r_>=\max\{r,r'\}$.

Alternatively, one can also write the following integral representation for the Green's function:

$$G_{k,l}(r,r')=\frac{2}{\pi}\int_0^\infty dq\,\frac{\hat{j}_l(qr)\hat{j}_l(qr')}{k^2-q^2}, \tag{9}$$

which can be proven to fulfill Eq. (3) by direct substitution and using the ordinary differential equation satisfied by the spherical Bessel functions $j_l(qr)$. To furnish the proof one has to apply the integral representation of the Dirac δ function

$$\delta(r-r')=\frac{2}{\pi}\int_0^\infty dq\ \hat{j}_l(qr)\,\hat{j}_l(qr'). \tag{10}$$

Notice in Eq. (9) the symbol $\fint$, denoting the Cauchy principal value of the integral, needed because of the simple pole at $q=k$ in the integrand.

III. GENERAL FORMALISM OF THE BETHE–GOLDSTONE EQUATION

The BG equation is also known as the *in-medium* scattering equation. It describes the quantum-mechanical state of two particles (fermions) interacting through a potential V when they are immersed in a medium. The medium prevents them from being scattered into filled levels below the Fermi momentum k_F, thus fulfilling the Pauli exclusion principle.

In operator form the BG equation reads

$$G(E)=V+V\frac{Q}{E-H_0}G(E), \tag{11}$$

where $G(E)$ is the G matrix, H_0 is the unperturbed Hamiltonian of the problem, E is the energy of the correlated pair, and Q is the Pauli-blocking operator, which projects out of the Fermi sphere.

In the case of nuclear matter, the unperturbed Hamiltonian H_0 corresponds to the kinetic energy and its eigenfunctions are the single-particle plane-wave solutions with definite momentum, $|\mathbf{p}_1\mathbf{p}_2\rangle$.

If we take matrix elements between pairs of plane-wave states in Eq. (11), and factor out the center of mass (c.m.), then we obtain

$$\langle\mathbf{k}'|G(E)|\mathbf{k}\rangle=\langle\mathbf{k}'|V|\mathbf{k}\rangle+\int\frac{d^3\mathbf{q}}{(2\pi)^3}\langle\mathbf{k}'|V|\mathbf{q}\rangle\frac{Q(\mathbf{q},\mathbf{P})}{E-\mathbf{q}^2/(2\mu)}\times\langle\mathbf{q}|G(E)|\mathbf{k}\rangle, \tag{12}$$

where $\mathbf{k}$ is the relative momentum of the pair and $\mu=\frac{M_N}{2}$ is the reduced mass of the NN pair. The Pauli-blocking operator $Q(\mathbf{q},\mathbf{P})=\theta(|\mathbf{P}/2+\mathbf{q}|-k_F)\,\theta(|\mathbf{P}/2-\mathbf{q}|-k_F)$ depends on the total momentum of the pair, $\mathbf{P}$, and it breaks the rotational invariance of the BG equation, with an explicit dependence on the angle between the total momentum, $\mathbf{P}$, and the relative momentum, $\mathbf{q}$. This is known to generate a mixing among all partial waves [58]. Since the early days, Brueckner proposed the so-called averaging procedure [59]. An exact treatment of the Pauli operator was discussed in Refs. [60,61], bringing about non-negligible and attractive contributions to the binding energy. Recently, a three-dimensional approach was proposed to deal with the problem [62] and the implications for in-medium nucleon-nucleon cross sections were analyzed [63].

In the independent pair approximation [64] the BG equation provides a well-defined way to compute the effective two-body operator, the G matrix, which is appropriate to be used in perturbation theory instead of the bare NN interaction. In this work we solve the BG equation in the simplest case, i.e., for total momentum $\mathbf{P}=\mathbf{0}$, corresponding to a pair of back-to-back nucleons interacting in the medium. In this case the influence of SRC in the nuclear dynamics is expected to be the largest. The general case of the $\mathbf{P}\neq\mathbf{0}$ will be discussed in future work.

A. Bethe–Goldstone equation in integral form

The advantage of the integral representation of the scattering problem sketched in Sec. II is that the BG equation for a back-to-back correlated pair is straightforwardly obtained. In fact we just replace the lower limit in the Green's function integral representation, Eq. (9), by the Fermi momentum k_F,

$$G_{k,l}(r,r')\to\widetilde{G}_{k,l}(r,r')=\frac{2}{\pi}\int_{k_F}^\infty dq\frac{\hat{j}_l(qr)\hat{j}_l(qr')}{k^2-q^2}. \tag{13}$$

This kernel integral could be computed analytically in terms of the integral cosine and sine functions, $\mathrm{Ci}(x)$ and $\mathrm{Si}(x)$, but the expressions are a bit cumbersome for practical work. On the other hand, this integral is poorly converging numerically, although it can be handled with quadrature rules of Levin's type [65,66]. A convenient, alternative approach requires transforming the above integral as follows:

$$\begin{aligned}\widetilde{G}_{k,l}(r,r')&=\frac{2}{\pi}\int_0^\infty dq\frac{\hat{j}_l(qr)\hat{j}_l(qr')}{k^2-q^2}-\frac{2}{\pi}\int_0^{k_F}dq\frac{\hat{j}_l(qr)\hat{j}_l(qr')}{k^2-q^2}\\&=\frac{1}{k}\hat{j}_l(kr_<)\hat{y}_l(kr_>)-\frac{2}{\pi}\int_0^{k_F}dq\frac{\hat{j}_l(qr)\hat{j}_l(qr')}{k^2-q^2}.\end{aligned} \tag{14}$$

Note that in the first line of the above equation *both* integrals contain the Cauchy principal value so that the singularity at the pole $q=k$ cancels exactly. Thus, we are left with an integral with bounded limits, 0 and k_F. The Cauchy principal value can

be implemented by splitting the whole integral into different intervals, below and above the pole at $q = k$, and integrating symmetrically around this pole with a finite ϵ width and finally ensuring numerical convergence while taking the limit $\epsilon \to 0$. We have checked that both procedures yield numerically compatible results.

The analogous equation to Eq. (2) for the BG problem in the coupled-channels case amounts to replace the free Green's function by the medium one, $G \to \tilde{G}$, thus giving

$$\widetilde{u}_{k,l}(r) = \hat{j}_l(kr) + \int_0^\infty dr'\, \widetilde{G}_{k,l}(r,r') \sum_{l'} U_{l,l'}(r')\, \widetilde{u}_{k,l'}(r'), \tag{15}$$

where the symbol $\widetilde{u}_{k,l}(r)$ stands for the reduced relative wave function of a correlated nucleon pair.

For example, if we write Eq. (15) for the ${}^3S_1$–${}^3D_1$ coupled-channels case (the deuteron-like configuration) we have to solve the system of two integral equations

$$\widetilde{u}_{k,0}(r) = \hat{j}_0(kr) + \int_0^\infty dr'\, \widetilde{G}_{k,0}(r,r')[U_{0,0}(r')\, \widetilde{u}_{k,0}(r') + U_{0,2}(r')\, \widetilde{u}_{k,2}(r')], \tag{16}$$

$$\widetilde{u}_{k,2}(r) = \hat{j}_2(kr) + \int_0^\infty dr'\, \widetilde{G}_{k,2}(r,r')[U_{2,0}(r')\, \widetilde{u}_{k,0}(r') + U_{2,2}(r')\, \widetilde{u}_{k,2}(r')], \tag{17}$$

with analogous expressions for the other coupled partial waves.

B. The coarse-grained Bethe–Goldstone equation

In this section we specify a particular high-quality representation of the NN potential. For the purposes of this work, we consider the coarse-grained δ-shell Granada potential of Refs. [51,52]. We remind that the parameters of this δ-shell potential were fitted to reproduce a statistically significant selection of 6713 np- and pp-scattering data for $T_{\rm LAB} \leqslant 350$ MeV with $\chi^2/\nu = 1.04$ and providing the most accurate description of NN scattering to date.[1] In a first approximation we will discard all long-distance effects, such as CD-OPE or Coulomb, which in the Granada potential start at 3 fm. These are crucial for the scattering data analysis but will have little influence on the SRC.[2]

In the δ-shell representation, the reduced NN potential is written as a sum of Dirac δs sampled at discrete points

$$U_{l,l'}(r) = 2\mu V_{l,l'}(r) = \sum_{i=1}^{N_\delta} (\lambda_i)^{SJ}_{l,l'}\, \delta(r - r_i), \tag{18}$$

where the strengths $(\lambda_i)^{SJ}_{l,l'}$ depend on the total spin (S) and total angular momentum (J) of each (coupled or not) partial wave ${}^{2S+1}L_J$. For subsequent discussions in this paper we label the reduced wave function, $\widetilde{u}_{k,l}(r)$, also with the SJ quantum numbers that unambiguously identify the partial wave. In this work we use the values of the parameters $(\lambda_i)^{SJ}_{l,l'}$ quoted in Table I of Ref. [51], with $N_\delta = 5$, and $r_i = \Delta r\, i = 0.6i$ fm.

With the coarse-grained potential of Eq. (18), the integrations in Eq. (15) can be immediately performed, resulting in

$$\widetilde{u}^{SJ}_{k,l}(r) = \hat{j}_l(kr) + \sum_{i=1}^{N_\delta} \widetilde{G}_{k,l}(r,r_i) \sum_{l'} (\lambda_i)^{SJ}_{l,l'}\, \widetilde{u}^{SJ}_{k,l'}(r_i). \tag{19}$$

To solve the BG equation in this representation we write the above equation for the grid points, $r = r_j$ ($j = 1,2,\ldots,N_\delta$), obtaining a linear system of N_δ equations where the unknowns correspond to the reduced wave functions at the grid points, $\widetilde{u}^{SJ}_{k,l}(r_i)$,

$$\widetilde{u}^{SJ}_{k,l}(r_j) = \hat{j}_l(kr_j) + \sum_{i=1}^{N_\delta} \widetilde{G}_{k,l}(r_j,r_i) \sum_{l'} (\lambda_i)^{SJ}_{l,l'}\, \widetilde{u}^{SJ}_{k,l'}(r_i). \tag{20}$$

In this way we have reduced the BG problem from an integral equation (15) to a linear system of algebraic equations (20). This linear system can be easily solved by standard matrix inversion methods. Once we know the solutions at the grid points, $\widetilde{u}^{SJ}_{k,l}(r_i)$, we can determine the wave function at any other point, r, by using Eq. (19). Note that the very nature of the potential does imply a wave function with "spikes" in between the grid points, with no physical consequences, as it will be shown below.

C. NN high-momentum components

In the last section we have solved the BG equation in coordinate space through a partial wave expansion of the relative wave function for total momentum of the nucleon pair $\mathbf{P} = \mathbf{0}$. This provides the spatial wave function of a correlated two-nucleon pair in back-to-back configuration for initial relative momentum of the pair equal to $\mathbf{k}$. The BG equation naturally introduces high-momentum components with $p > k_F$ in this solution. In this section we will compute these components by Fourier transform.

The spins of the nucleon pair can be coupled to total spin $S = 0,1$. We start with the well-known expression for a spinless plane wave (Rayleigh expansion),

$$e^{i\mathbf{k}\cdot\mathbf{x}} = 4\pi \sum_{l,m} i^l\, j_l(kr) Y^*_{l,m}(\hat{\mathbf{k}}) Y_{l,m}(\hat{\mathbf{x}}), \quad \text{with} \quad r = |\mathbf{x}|. \tag{21}$$

Its generalization to the spin-S case is

$$e^{i\mathbf{k}\cdot\mathbf{x}} \chi_{SM_s} = 4\pi \sum_{l,m} i^l\, j_l(kr) Y^*_{l,m}(\hat{\mathbf{k}}) \times \sum_{J,M} \langle lmSM_s|JM\rangle \mathcal{Y}_{lSJM}(\hat{\mathbf{x}}), \tag{22}$$

where χ_{SM_s} is an eigenspinor with spin quantum numbers (S,M_s), and the functions $\mathcal{Y}_{lSJM}(\hat{\mathbf{x}})$ are the couplings of the

[1] We have recently improved the description in Ref. [67] $\chi^2/\nu = 1.025$ by fitting also the pion-nucleon coupling constants. We will not consider this new fit in this work.

[2] In fact, in the ${}^1S_0$ channel both effects are comparable since $V_C(r_c) = e^2/r_c \sim 0.5$ MeV and $V_{\rm OPE}(r_c) = -f^2 e^{-m_\pi r_c}/r_c \sim -0.5$ MeV for $f^2 = 0.0763(1)$ [67].

the spherical harmonics with the spinors χ_{SM_s} to total angular momentum J,

$$\mathcal{Y}_{lSJM}(\hat{\mathbf{p}}) = \sum_{m',M'_s} \langle lm'SM'_s|JM\rangle Y_{l,m'}(\hat{\mathbf{p}})\,\chi_{SM'_s}. \tag{23}$$

The boundary conditions of the BG equation imply that, asymptotically, the BG wave function converges to the free plane wave. Therefore we perform a partial wave expansion similar to Eq. (22),

$$\Psi^{\rm BG}_{\mathbf{k},SM_s}(\mathbf{x}) = 4\pi \sum_{lmJM} i^l \frac{\widetilde{u}^{SJ}_{k,l}(r)}{kr} Y^*_{l,m}(\hat{\mathbf{k}}) \times \langle lmSM_s|JM\rangle \mathcal{Y}_{lSJM}(\hat{\mathbf{x}}). \tag{24}$$

The normalization for the reduced wave function chosen in Eqs. (15) and (19) automatically ensures that Eq. (24) approaches to Eq. (22) when $r \to \infty$. The labels $(\mathbf{k}, SM_s)$ on the BG wave function indicate that, asymptotically, this correlated relative wave function converges to a free plane wave with the nucleons spins coupled to total spin S and third-component M_s.

To describe the high-momentum components of the correlated NN pair, we calculate the Fourier transform of Eq. (24)

$$\Phi^{\rm BG}_{\mathbf{k},SM_s}(\mathbf{p}) = \int \frac{d^3\mathbf{x}}{(2\pi)^3}\, e^{-i\mathbf{p}\cdot\mathbf{x}}\, \Psi^{\rm BG}_{\mathbf{k},SM_s}(\mathbf{x}). \tag{25}$$

By expanding the complex exponential with the complex conjugate of Eq. (21), and after substitution of Eq. (24) into (25), one can integrate over the angular variables of $d^3\mathbf{x}$ with the aid of the identity

$$\int d\Omega_{\hat{\mathbf{x}}}\, Y^*_{l',m'}(\hat{\mathbf{x}})\, \mathcal{Y}_{lSJM}(\hat{\mathbf{x}}) = \delta_{l,l'} \sum_{M'_s} \langle lm'SM'_s|JM\rangle \chi_{SM'_s}. \tag{26}$$

The Kronecker δ, $\delta_{l,l'}$, allows to perform one of the partial sums implicit in Eq. (25), producing as final result

$$\Phi^{\rm BG}_{\mathbf{k},SM_s}(\mathbf{p}) = \sum_{lm}\sum_{JM} \phi_{k,lSJ}(p) Y^*_{l,m}(\hat{\mathbf{k}}) \langle lmSM_s|JM\rangle \times \mathcal{Y}_{lSJM}(\hat{\mathbf{p}}), \tag{27}$$

where

$$\phi_{k,lSJ}(p) \equiv \frac{2}{\pi}\int_0^\infty dr\, r^2\, j_l(pr)\, \frac{\widetilde{u}^{SJ}_{k,l}(r)}{(kr)}, \tag{28}$$

is the "radial" wave function in momentum space for the partial wave $^{2S+1}L_J$. This "radial" function is proportional to the probability amplitude of finding a correlated two-nucleon pair, with initial relative momentum k, having relative momentum p in each partial wave.

To perform the integral in expression (28) we note that the reduced wave function, $\widetilde{u}^{SJ}_{k,l}(r)$, fulfills equation (19). Therefore, on substituting Eq. (19) into Eq. (28) and by using the analogous expression to Eq. (10) in momentum space, we obtain

$$\phi_{k,lSJ}(p) = \frac{2}{\pi}\left\{\frac{\pi}{2pk}\delta(p-k) + \frac{1}{k}\sum_{i=1}^{N_\delta}\sum_{l'}(\lambda_i)^{SJ}_{l,l'}\,\widetilde{u}^{SJ}_{k,l'}(r_i) \times \int_0^\infty dr\, r\, j_l(pr)\,\widetilde{G}_{k,l}(r,r_i)\right\}. \tag{29}$$

Finally, substituting Eq. (13) into the above expression (29), permuting the order of the integrations between r and q variables, and using again the orthogonality relation, Eq. (10), of the spherical Bessel functions, we obtain the result

$$\phi_{k,lSJ}(p) = \frac{1}{pk}\delta(p-k) + \frac{2}{\pi k}\frac{\theta(p-k_F)}{k^2-p^2} \times \sum_{i=1}^{N_\delta} r_i\, j_l(pr_i) \sum_{l'}(\lambda_i)^{SJ}_{l,l'}\,\widetilde{u}^{SJ}_{k,l'}(r_i), \tag{30}$$

where the first term corresponds to the low-momentum component of the correlated two-nucleon state, while the second term explicitly incorporates the condition $p > k_F$ through the step function. Therefore, it is the high-momentum component of the correlated two-nucleon system. An expression similar to Eq. (30) was provided in Eq. (44) of Ref. [55] for the high-momentum components of the $^1S_0$ partial wave, except for an overall normalization factor. Its origin has to be traced back to the different normalizations used in the partial-wave expansions of the BG wave function. Here we have developed the general proof for all partial waves using a different representation of the BG equation.

Equation (30) is the main formula of this work. The high-momentum components of the partial wave functions contain a common factor k^2-p^2 in the denominator, modulated by a linear combination of spherical Bessel functions evaluated at the points pr_i. This simple, analytical dependence represents an important, universal feature of the SRC. The information of the NN interaction is encoded here in the quantities $\sum_{l'}(\lambda_i)^{SJ}_{l,l'}\widetilde{u}^{SJ}_{k,l'}(r_i)$. Another feature of the SRC is that the NN potential parameters always appear multiplied by the BG wave function evaluated at the grid points.

In the next section we will present numerical results for the BG partial wave functions and for the high-momentum distribution. This distribution is proportional to the probability density for an initial pair with relative momentum $\mathbf{k}$ and total spin $|S,M_s\rangle$ of being found after the interaction in a state of relative momentum p in any direction. This is obtained by taking the squared modulus of the BG wave function $\Phi^{\rm BG}_{\mathbf{k},SM_s}(\mathbf{p})$, given by Eq. (27), and integrating over all the directions of $\hat{\mathbf{p}}$,

$$\int d\Omega_{\hat{\mathbf{p}}}\left|\Phi^{\rm BG}_{\mathbf{k},SM_s}(\mathbf{p})\right|^2 = \sum_{l}\sum_{m,m'}\sum_{J,M}|\phi_{k,lSJ}(p)|^2\, Y_{l,m'}(\hat{\mathbf{k}}) \times Y^*_{l,m}(\hat{\mathbf{k}})\langle lm'SM_s|JM\rangle\langle lmSM_s|JM\rangle, \tag{31}$$

where we have exploited the orthonormal properties of the spin spherical harmonics

$$\int d\Omega_{\hat{\mathbf{p}}}\, \mathcal{Y}^*_{l'S'J'M'}(\hat{\mathbf{p}})\, \mathcal{Y}_{lSJM}(\hat{\mathbf{p}}) = \delta_{l',l}\, \delta_{S',S}\, \delta_{J',J}\, \delta_{M',M}. \quad (32)$$

Notice that Eq. (31) still depends on the angles of $\hat{\mathbf{k}}$. No further simplification is possible in expression (31) unless we average it over all the possible directions of $\hat{\mathbf{k}}$. This average provides the probability density of a correlated nucleon pair with initial relative momentum k (in any direction) and total spin $|S,M_s\rangle$ to be found after the interaction in a state of relative motion with momentum p (in any direction) as well. Using the orthogonality property of the spherical harmonics, we can perform the angular integration, obtaining

$$\frac{1}{4\pi}\int d\Omega_{\hat{\mathbf{k}}} \int d\Omega_{\hat{\mathbf{p}}} \left|\Phi^{\rm BG}_{\mathbf{k},SM_s}(\mathbf{p})\right|^2 = \frac{1}{4\pi}\sum_{l,J} |\phi_{k,lSJ}(p)|^2 \sum_{m,M} \langle lmSM_s|JM\rangle \langle lmSM_s|JM\rangle, \quad (33)$$

$$= \frac{1}{4\pi}\frac{1}{2S+1}\sum_{l,J}(2J+1)|\phi_{k,lSJ}(p)|^2, \quad (34)$$

where we have used the symmetry property of the Clebsch–Gordan coefficients

$$\langle lmSM_s|JM\rangle = (-1)^{l-m}\sqrt{\frac{2J+1}{2S+1}}\langle lmJ-M|S-M_s\rangle. \quad (35)$$

It is worth noting that the sum over (l,J) quantum numbers in expression (34) is not truly independent, as it only runs over the pairs of values compatible with the coupling of angular momenta $[l\otimes S]_J$, and with the antisymmetry of the whole wave function for a system of two identical nucleons, as in pp or nn configurations.

It should also be remarked that expression (34) does not depend at all on the spin third-component quantum number M_s. Therefore, if we sum Eq. (34) over all possible M_s values, the factor $(2S+1)$ in the denominator of the right-hand side of Eq. (34) cancels out.

To get rid of the low-momentum component (the piece with the δ function) in Eq. (30), when applying Eq. (34) we restrict the relative momentum p to be greater than the Fermi momentum k_F. With this restriction we avoid bothering about the treatment of the square of a δ function distribution, because the initial relative momentum k is always below k_F ($k<k_F$).

Using the results discussed above one can compute the BG wave function corresponding to a nucleon pair with initial relative momentum $\mathbf{k}$ and spin components m_1,m_2. This is obtained as an expansion in terms of BG wave functions of coupled pairs

$$\widetilde{\Phi}^{\rm BG}_{\mathbf{k},m_1m_2}(\mathbf{p}) = \sum_{S,M_s}\left\langle \frac{1}{2}m_1\frac{1}{2}m_2|SM_s\right\rangle \Phi^{\rm BG}_{\mathbf{k},SM_s}(\mathbf{p}). \quad (36)$$

Note that the probability averaged over spins verifies

$$\frac{1}{4}\sum_{m_1,m_2}\left|\widetilde{\Phi}^{\rm BG}_{\mathbf{k},m_1m_2}(\mathbf{p})\right|^2 = \frac{1}{4}\sum_{S,M_s}\left|\Phi^{\rm BG}_{\mathbf{k},SM_s}(\mathbf{p})\right|^2, \quad (37)$$

where the factor $\frac{1}{4}$ reflects the two possible spin states for each nucleon.

IV. NUMERICAL RESULTS

In this section we provide results for the solution of the BG equation of a nucleon pair in nuclear matter. All the calculations have been done for a Fermi momentum of $k_F = 250$ MeV. Unless otherwise specified, we will show results for a fixed value $k = 140$ MeV/c of the relative momentum of the pair. The reason to choose this specific value for the relative momentum of the nucleon pair is twofold: First, it represents an intermediate value for the allowed relative momenta between 0 and k_F; and, second, it is also one of the values considered in our previous work [55], where we only treated the $^1S_0$ partial wave. In this way, it will provide a more direct comparison with the results already obtained in Ref. [55], at least for the $^1S_0$ channel.

Finally, it is worth warning the reader that the GR potential is determined by the strengths at the grid points $(\lambda_i)^{SJ}_{l,l'}$ for all the partial waves appearing in Table I of Ref. [51].

A. BG solutions on the grid points

In the case of total spin $S=0$ we solve the linear system (20). The unknowns are the values of the wave function at the grid points $\widetilde{u}^{SJ}_{k,l}(r_i)$ for $J=l$, and $l=0,1,2,3$. Note that our grid consist simply in the five points $r_i = 0.6, 1.2, 1.8, 2.4$, and 3 fm. Thus the solution of the BG in this case only requires us to invert a 5×5 real matrix. In the case $S=1$, the $l=J$ partial waves are uncoupled so they also require us to invert a 5×5 matrix. However, the $l=J-1$ and $l=J+1$ multipoles are coupled and this implies to solve a system of 10 linear equations.

Thus the GR potential allows us to solve the BG equation at minor computational cost. The only difficulties are to perform numerically the one-dimensional integral in Eq. (14) to compute the Green's function and to invert at most a 10×10 matrix for each pair of coupled multipoles. Note that this extreme simplification appears only because we have coarse-grained the potential with a few grid points. Using instead a more general local NN potential would require to use a very fine grain, with $N_\delta > 100$ points, increasing the dimensionality of the matrices to invert. To solve the BG equation with more than 100 grid points would require highly intensive computation, thus losing the practical advantages of the GR potential.

In Fig. 1 we show the correlated reduced wave functions $\widetilde{u}^{SJ}_{k,l}(r_i)$ on the grid points (dots on the plot) used in the matrix inversion and for each one of the uncoupled channels appearing in Table I of Ref. [51].

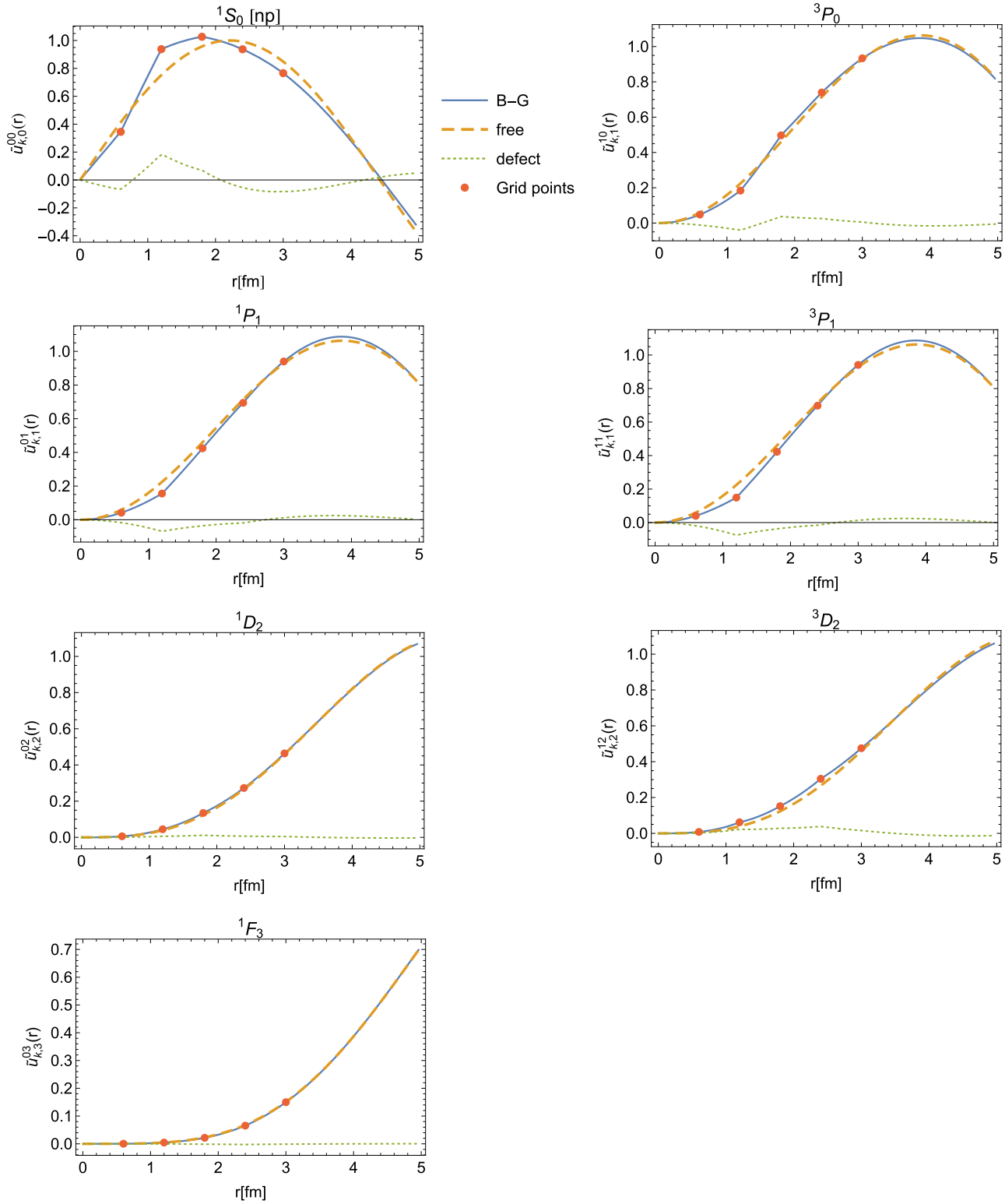

FIG. 1. BG wave functions $\widetilde{u}^{SJ}_{k,l}(r)$ for the uncoupled NN partial waves. We also display the free solution $\hat{j}_l(kr)$ in dashed style and the defect wave function $\Delta\widetilde{u}^{SJ}_{k,l}(r) \equiv \widetilde{u}^{SJ}_{k,l}(r) - \hat{j}_l(kr)$ as dotted lines. The calculations have been done for a relative momentum of the pair $k = 140$ MeV.

B. BG wave functions in coordinate space

As discussed above, knowledge of the wave function at the grid points allows us to reconstruct the full wave function using the BG equation. In Fig. 1 the correlated wave function is compared with the free solution $\hat{j}_l(kr)$. We also show the defect wave function, defined as the difference between correlated

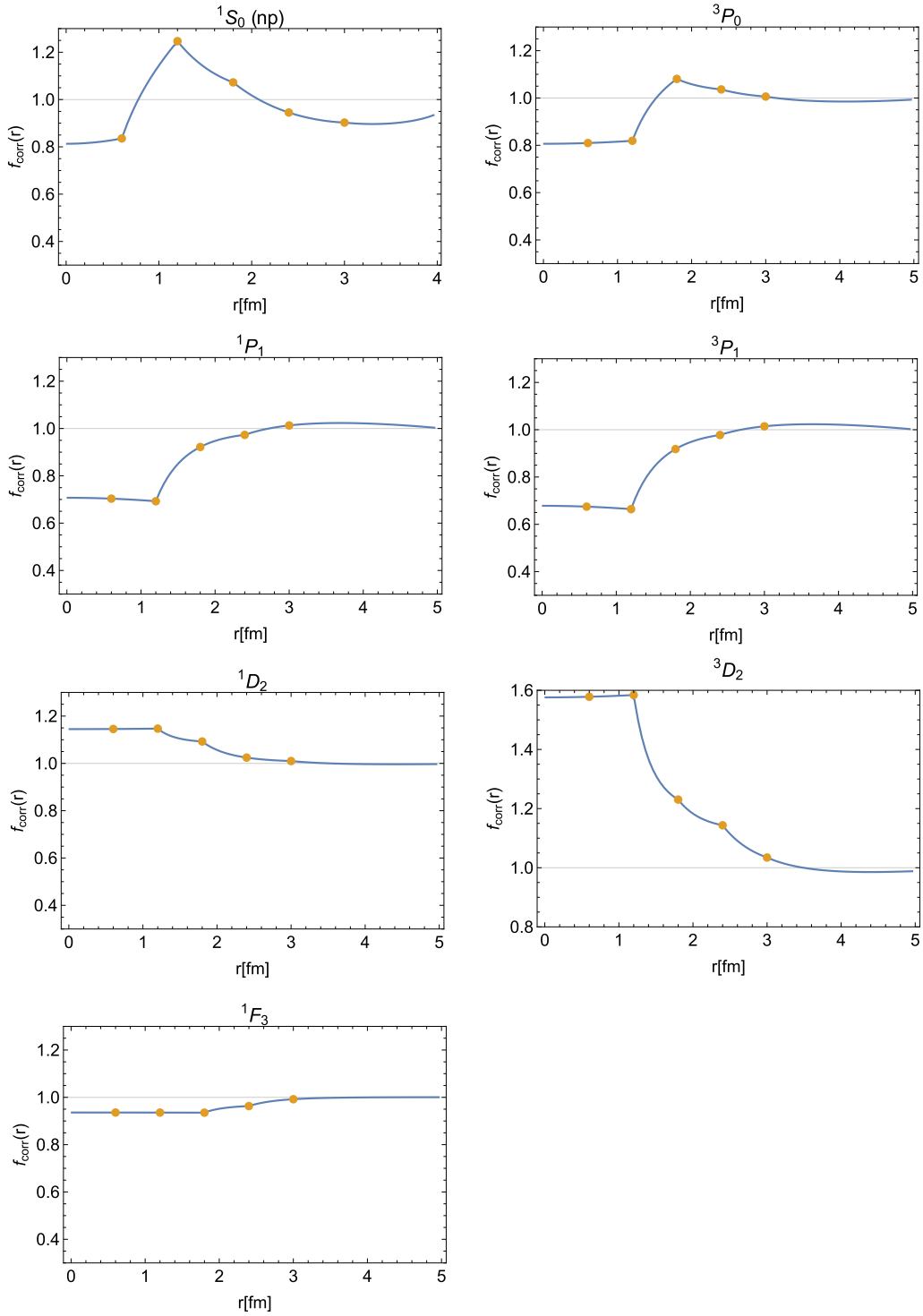

FIG. 2. Correlation function $f_{\rm corr}(r) \equiv \frac{\widetilde{u}^{SJ}_{k,l}(r)}{\hat{j}_l(kr)}$ for each uncoupled NN partial wave. The calculations have been done for $k = 140$ MeV.

and uncorrelated waves,

$$\Delta\widetilde{u}^{SJ}_{k,l}(r) \equiv \widetilde{u}^{SJ}_{k,l}(r) - \hat{j}_l(kr). \tag{38}$$

As we see the effect of the interaction is to modify the relative wave function of the pair for short to intermediate distances. For large distances the wave function becomes equal to the free one without any phase shift. The SRC effects are more prominent for the low-L partial waves, S, P, and D especially. The interaction effect is largest for the S wave and decreases with the relative angular momentum. For $l = 3$ the defect wave function is very small and cannot be seen in the scale of the figure. When the angular momentum

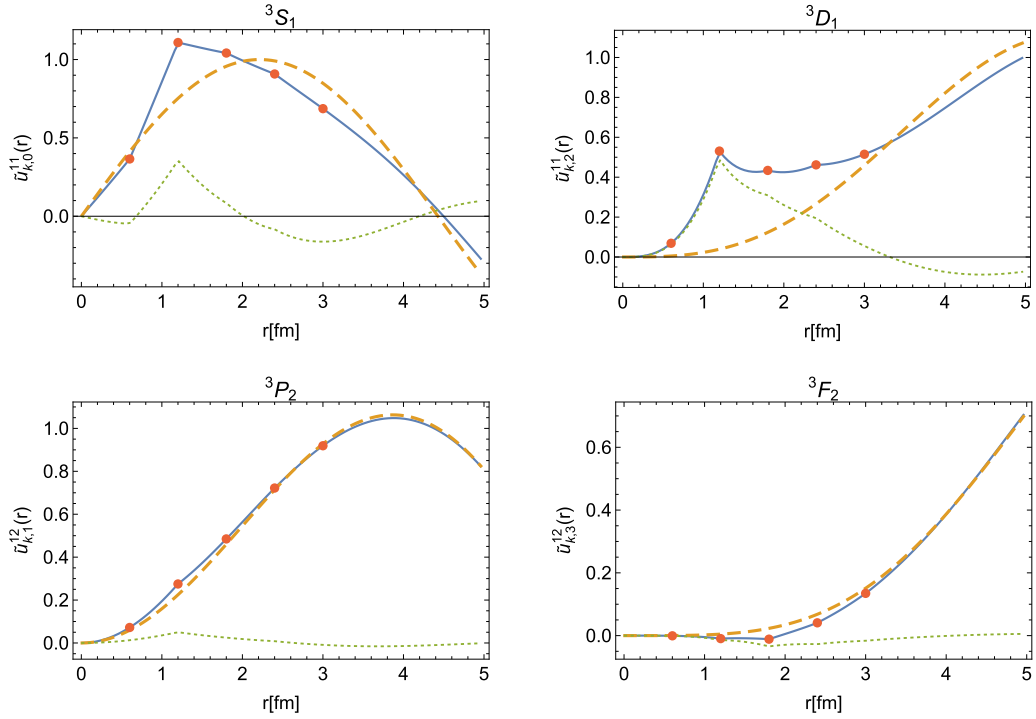

FIG. 3. BG wave functions $\widetilde{u}^{SJ}_{k,l}(r)$ for the coupled NN partial waves $^3S_1$–$^3D_1$ and $^3P_2$–$^3F_2$. We also display the free solution $\hat{j}_l(kr)$ in dashed style, and the defect wave function $\Delta\widetilde{u}^{SJ}_{k,l}(r)$ as dotted lines. The calculations have been done for a relative momentum of the pair $k = 140$ MeV.

increases the nucleons are far apart and the SRC effects go away. This is due to the centrifugal barrier, which is more repulsive for peripheral partial waves and prevents the two nucleons to approach each other at short distances, where the short-range potential is noticeable. Besides, direct inspection of Table I of Ref. [51] reveals that for growing angular momentum the inner δ shells (below the centrifugal barrier) are vanishing.

The results for the $^1S_0$ (np) partial wave can be compared to those corresponding to Fig. 3(d) of Ref. [55]. They are similar but not equal because the δ-shell parameters used in Ref. [55] are not the same as here. Indeed, in Ref. [55], the strengths of the δ shells in this partial wave were adjusted to reproduce the same phase shifts as the AV18 potential [48] up to a certain energy. The strengths used in the present work were simultaneously fitted in a PWA to NN-scattering data [51–53]. In addition, here we consider five δ shells, while Fig. 3(d) of Ref. [55] was done with seven δ shells.

C. Correlation functions

In Fig. 2 we plot the results for the correlation function, defined as the ratio between the BG and the free wave functions,

$$f_{\rm corr}(r) \equiv \frac{\widetilde{u}^{SJ}_{k,l}(r)}{\hat{j}_l(kr)}, \tag{39}$$

for each one of the uncoupled NN partial waves shown in Fig. 1, with the same choice for the relative momentum $k = 140$ MeV. The correlation function approaches unity, after a few oscillations, at long distances ($r \gtrsim 3$ fm) where the effects of the short-range NN potential are becoming more and more negligible. The significant deviation from unity for the correlation function occurs at short distances, where the NN potential is present.

An important feature that can be observed from Fig. 2 is that the correlation function is quite constant for the shortest distances, below the range of the first nonvanishing delta-shell strength $(\lambda_i)^{SJ}_{l,l}$, which occurs at different distances for each partial wave, as can be seen from the values quoted in Table I of Ref. [51]. Additionally, the sign of the first nonvanishing strength λ_i in each partial wave determines if the correlation function is larger or smaller than unity at the shortest distances, thus reflecting the attractive or repulsive nature of the potential in each channel, and the probability for the two correlated nucleons of being closer or farther relative to the uncorrelated situation. The first nonvanishing δ-shell strengths are positive in the S, P, and F channels of Fig. 2, while they are negative in the D partial waves. The correlation function is especially large at short distances for the $^3D_2$ channel as compared to the $^1D_2$ case, due to the much stronger attractive character of the first λ at 1.2 fm in the $^3D_2$ partial wave (cf. Table I of Ref. [51]).

Finally, if one compares the first panel of Fig. 2, corresponding to the $^1S_0$ (np) channel, with Fig. 4(b) of the analysis made in Ref. [55], one can observe that the tails of the correlation function for distances larger than 2 fm are extremely similar. However, the detailed structure of the inner region (below 2 fm) strongly depends on the strengths of the δ shells, which are different in both analyses. Notice that the correlation function below 0.5 fm in Fig. 4(b) of Ref. [55] is much more suppressed than here, indicating a harder core in the GR7 potential used

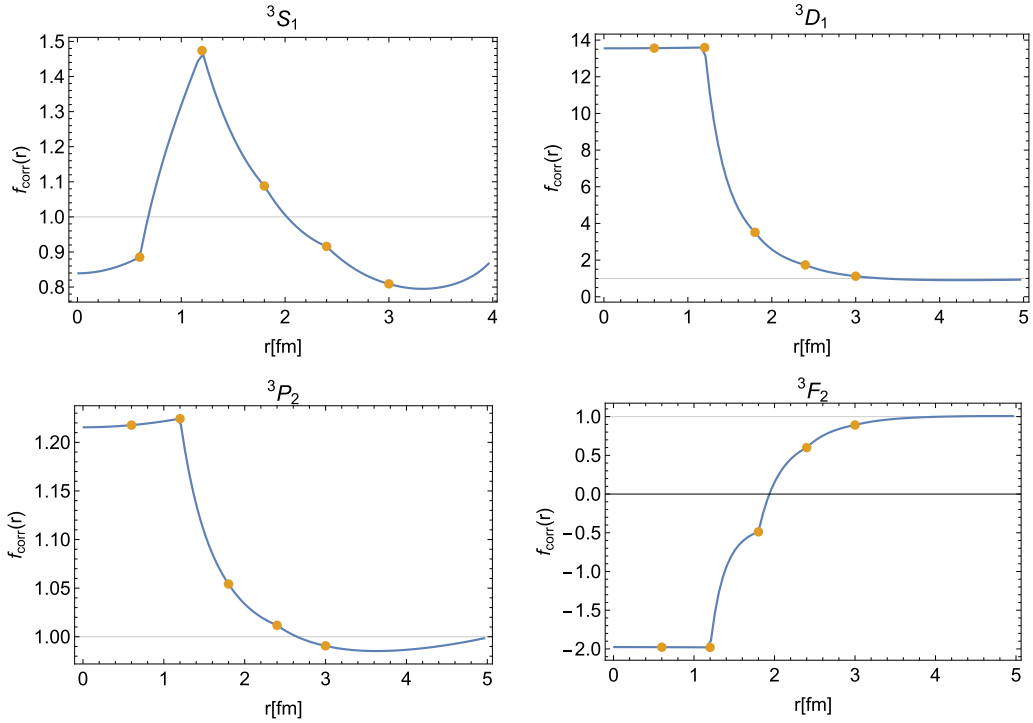

FIG. 4. Correlation function $f_{\rm corr}(r)$ for the coupled NN partial waves $^3S_1$–$^3D_1$ and $^3P_2$–$^3F_2$. The calculations have been done for $k = 140$ MeV.

there. That hardness in the potential produces appreciable differences in the description of the very high momentum components in the NN wave function [55].

D. Coupled channels

In Fig. 3 we show the analogous results to Fig. 1 for the coupled $^3S_1$–$^3D_1$ and $^3P_2$–$^3F_2$ partial waves. The corresponding strengths for the δ shells are taken from Table I in Ref. [51], where the nondiagonal strengths $(\lambda_i)^{SJ}_{l,l'}$ with $l \neq l'$ are labeled by ϵ_J. These results have been obtained by solving Eqs. (19) and (20) for relative momentum $k = 140$ MeV.

By comparing these coupled partial waves with their uncoupled counterparts (Fig. 1) we can observe that the short-distance distortion of the wave function is larger for coupled than for uncoupled channels, especially for the case $L = J + 1$, i.e., the $^3D_1$ and $^3F_2$ waves. Notice that the effect of SRC is less important for the $L = J - 1$ waves, $^3S_1$ and $^3P_2$, which are much more similar to their uncoupled counterparts (the $^1S_0$ and the P waves shown in Fig. 1). This very large effect of SRC in the coupled waves is produced to a large extent by the mixing of the $l = J - 1, J + 1$ partial waves by the tensor force operator appearing in the NN interaction. This makes sense, first, because we have seen in the uncoupled waves that the SRC effects are more important for low-L. Since the tensor force is also present in the uncoupled waves through its diagonal part, we conclude that the strong correlations seen in the $^3D_1$ channel must be due to its mixing with the $^3S_1$ channel via the nondiagonal matrix elements of the Hamiltonian.

The same kind of conclusions can be drawn from observing the results of Fig. 4 for the correlation functions of the coupled waves. The $^3S_1$ correlation function is similar in magnitude to the $^1S_0$ one. The $^3P_2$ correlation function is larger than one for short distances, reflecting an attractive force at short distances, similar in magnitude to the repulsion seen in the uncoupled P-waves. The correlation functions of the coupled waves $^3D_1$ and $^3F_2$ show the largest distortion of the wave function at short distances. The SRC effect is especially large in the $^3D_1$ wave. Notice that $f_{\rm corr}(r) \approx 14$ for distances below 1.2 fm. For the $^3F_2$ channel we have $f_{\rm corr}(r) \approx -2$. The huge SRC effect seen in the coupled waves $^3D_1$ and $^3F_2$ is in contrast to the much softer effect found for the D and F uncoupled partial waves seen in Fig. 2.

In order to understand the importance of the mixing between coupled partial waves, we switch off the nondiagonal δ-shell strengths, $(\lambda_i)^{SJ}_{l,l'} = 0$ for $l \neq l'$. With this trick, the BG equations in Eq. (20) get effectively uncoupled, and all partial waves can be solved separately. Note that with this trick we are artificially "amputating" the NN potential by neglecting the nondiagonal part of the tensor force but leaving intact its diagonal part. So, the diagonal part of the tensor force is still present in this calculation.

The results for the "uncoupled" $^3S_1$ and $^3D_1$ waves are shown in Fig. 5, where we plot the reduced wave function and the correlation function. By comparing this figure with the coupled case of Fig. 3 we observe that the distortion in the wave function due to the SRC almost disappears in the $^3D_1$ partial wave and gets much quenched in the $^3S_1$ channel. This is more clear evidence on the importance of mixing and,

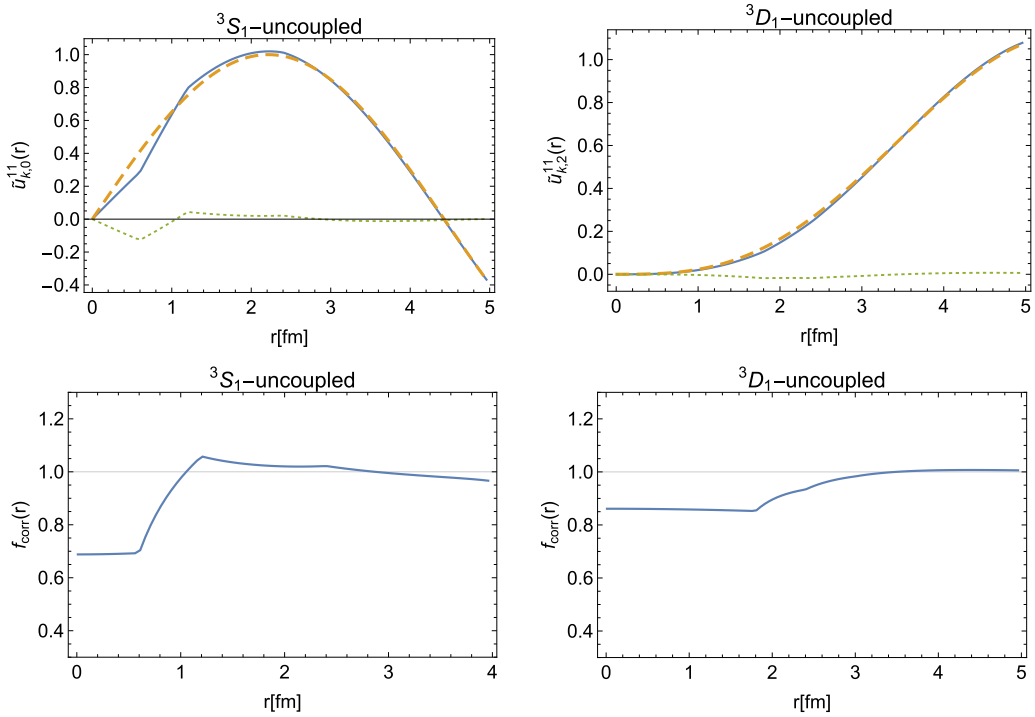

FIG. 5. Upper figures: BG wave functions $\widetilde{u}^{SJ}_{k,l}(r)$ for the NN partial waves $^3S_1$–$^3D_1$ treating them as fully uncoupled by switching off the nondiagonal strengths, $(\lambda_i)^{SJ}_{l,l'}$ with $l \neq l'$. Lines have the same meaning as in Figs. 1 and 3. Lower figures: Correlation function $f_{\rm corr}(r)$ for the same partial waves assuming no mixing between them. The calculations have been done for a relative momentum of the pair $k = 140$ MeV.

therefore, of the tensor force in the modification of the wave function at short distances (SRCs). The same conclusion can be drawn from the correlation function shown in the lower panel of Fig. 5: When the partial waves get uncoupled, the correlation functions at short distances are much closer to 1 than in the coupled case, where the full interaction is used.

Although not shown in this work, similar effects to those shown in Fig. 5 are observed in the $J = 2$ coupled channel if we switch off the nondiagonal δ-shell strengths and the linear system becomes uncoupled. The effects are relatively more significant in the $^3F_2$ wave, because it corresponds to the member of the coupled pair of partial waves with $L = J + 1$, as we already mentioned when discussing Fig. 3.

E. NN high-momentum components

In Fig. 6 we show the high-momentum components of the NN correlated wave function, given by the modulus squared of Eq. (30) for $p > k_F$. Figure 6(a) corresponds to the uncoupled channels already shown in Fig. 1 (except for the ^{1}P$_1$ wave, which is very similar to ^{3}P$_1$ and not shown), while in Fig. 6(b) we show the coupled partial waves depicted in Fig. 3.

Generally, in the uncoupled sector, the partial waves with higher probability of having high-momentum components are those of Fig. 1 that present the largest distortions (or defect wave functions) at short distances. Note that, for instance, for the $^1D_2$ and $^1F_3$ waves, the distortion effects are really small in Fig. 1, thus resulting in almost negligible contributions in the high-momentum tail of Fig. 6.

In the coupled sector, corresponding to Fig. 6(b), the most important high-momentum contributions are those of the $^3S_1$–$^3D_1$ coupled channels, which already showed the most prominent distortions at short distances in Fig. 3. Note the typical diffractive nodes appearing in the $^1S_0$ and $^3S_1$ partial waves for $p \approx 400$ MeV. The minimum of the $^3S_1$ wave will be highly suppressed by the addition of the relatively large momentum distribution of the $^3D_1$ wave. The minimum of the S wave momentum distribution is well known from previous studies [15,68] to appear for zero total momentum of the nucleon pair, as in the present work. In these other studies, this minimum was observed in the momentum distribution of pp pairs because these are predominantly found in a relative $^1S_0$ state (the $^3S_1$ is forbidden for pp pairs due to the Pauli principle restriction that the global wave function of the pair has to be antisymmetric). Notice that, although we have not shown here results for the $^1S_0$–pp channel, their δ-shell strengths are very similar to those of the $^1S_0$–np channel, and therefore the corresponding momentum distribution of the pair is very similar to that presented in Fig. 6(a) for the $^1S_0$–np state.

In order to understand in more depth the origin of the node in the $^3S_1$ partial wave and the effect of the mixing in the coupled $^3S_1$–$^3D_1$ channel, we show the results of Fig. 7. To properly apprehend the meaning of the different pieces contributing to the total high-momentum distribution of the $^3S_1$ and $^3D_1$ coupled partial waves, it is convenient to explicitly split the sum over l' in Eq. (30) in its diagonal part (with $l' = l$) and its off-diagonal part (with $l' \neq l$), for each one of these coupled

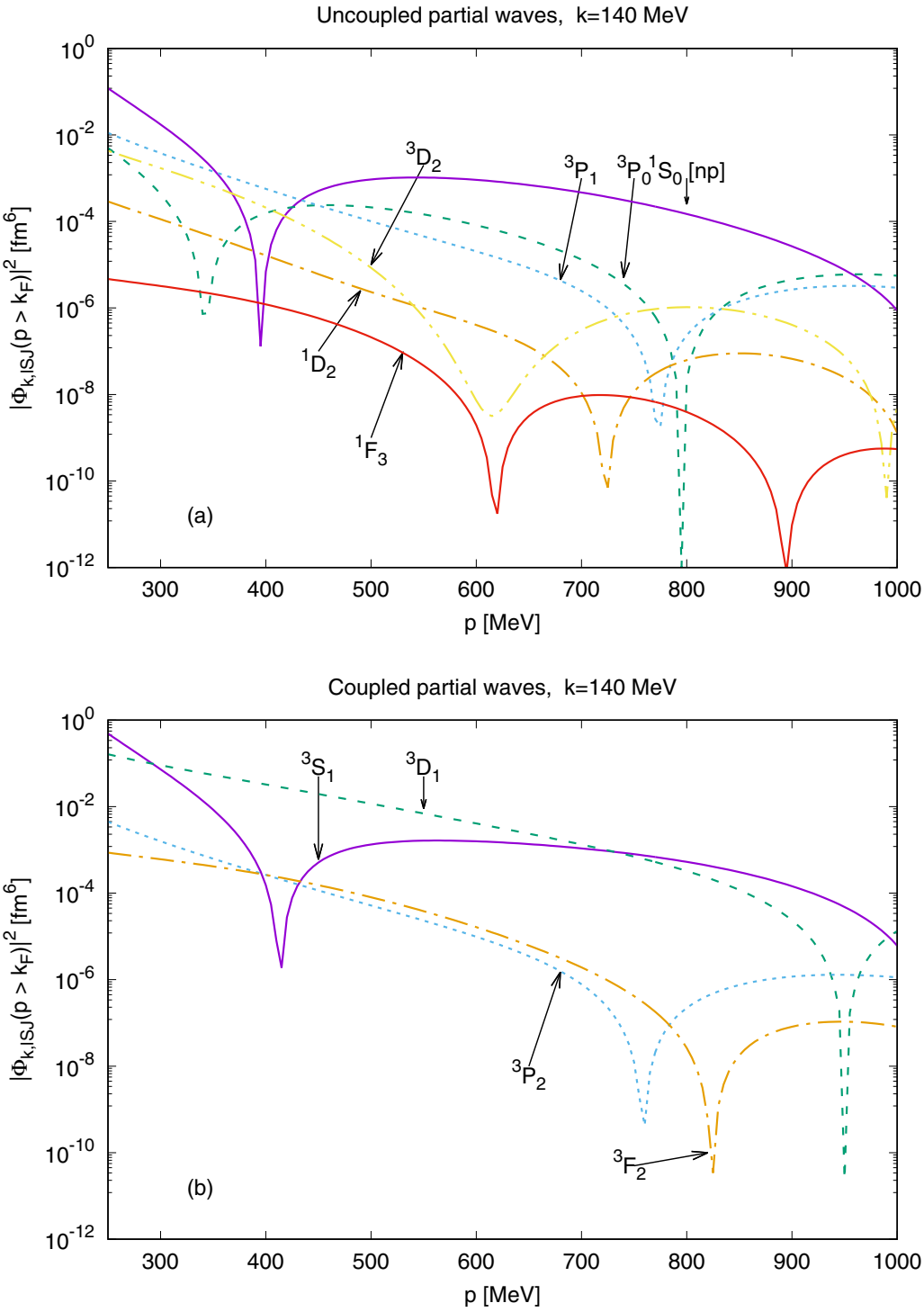

FIG. 6. NN high-momentum components $|\phi_{k,lSJ}(p)|^2$ in the correlated wave function, calculated for relative momentum of the nucleon pair $k = 140$ MeV. Panel (a) corresponds to the uncoupled NN partial waves, while panel (b) corresponds to the coupled ones. The high-momentum plotting region is restricted to $p > k_F$.

partial waves, thus obtaining:

$$\phi_{k,^3S_1}(p > k_F) = \frac{2}{\pi}\frac{1}{k}\frac{1}{k^2 - p^2}\left\{\underbrace{\sum_{i=1}^{N_\delta}\left\{r_i\, j_0(pr_i)(\lambda_i)_{\rm SS}\, \widetilde{u}_{k,^3S_1}(r_i)\right\}}_{\rm SS} + \underbrace{\sum_{i=1}^{N_\delta}\left\{r_i\, j_0(pr_i)(\lambda_i)_{\rm SD}\, \widetilde{u}_{k,^3D_1}(r_i)\right\}}_{\rm SD}\right\} = {\rm SS} + {\rm SD}, \quad (40)$$

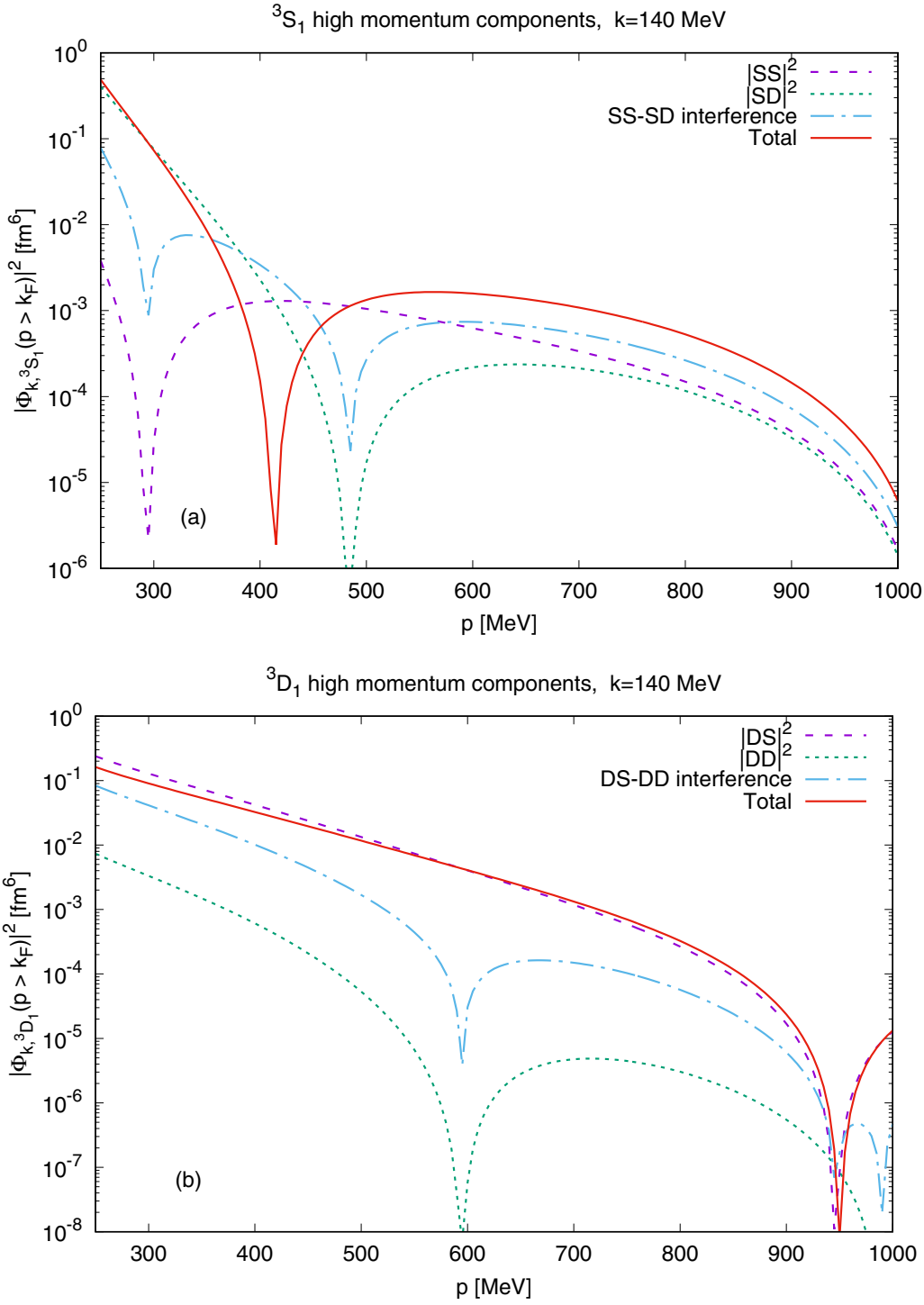

FIG. 7. (a) NN high-momentum components in the correlated wave function for the $^3S_1$ partial wave. (b) Same high-momentum components for the $^3D_1$ partial wave. Both calculations have been done for a relative momentum of the nucleon pair $k = 140$ MeV. The high-momentum plotting region is restricted to $p > k_F$.

and

$$\phi_{k,^3D_1}(p > k_F) = \frac{2}{\pi}\frac{1}{k}\frac{1}{k^2 - p^2}\left\{\underbrace{\sum_{i=1}^{N_\delta}\left\{r_i\, j_2(pr_i)(\lambda_i)_{\rm DS}\, \widetilde{u}_{k,^3S_1}(r_i)\right\}}_{\rm DS} + \underbrace{\sum_{i=1}^{N_\delta}\left\{r_i\, j_2(pr_i)(\lambda_i)_{\rm DD}\, \widetilde{u}_{k,^3D_1}(r_i)\right\}}_{\rm DD}\right\} = {\rm DS} + {\rm DD}, \quad (41)$$

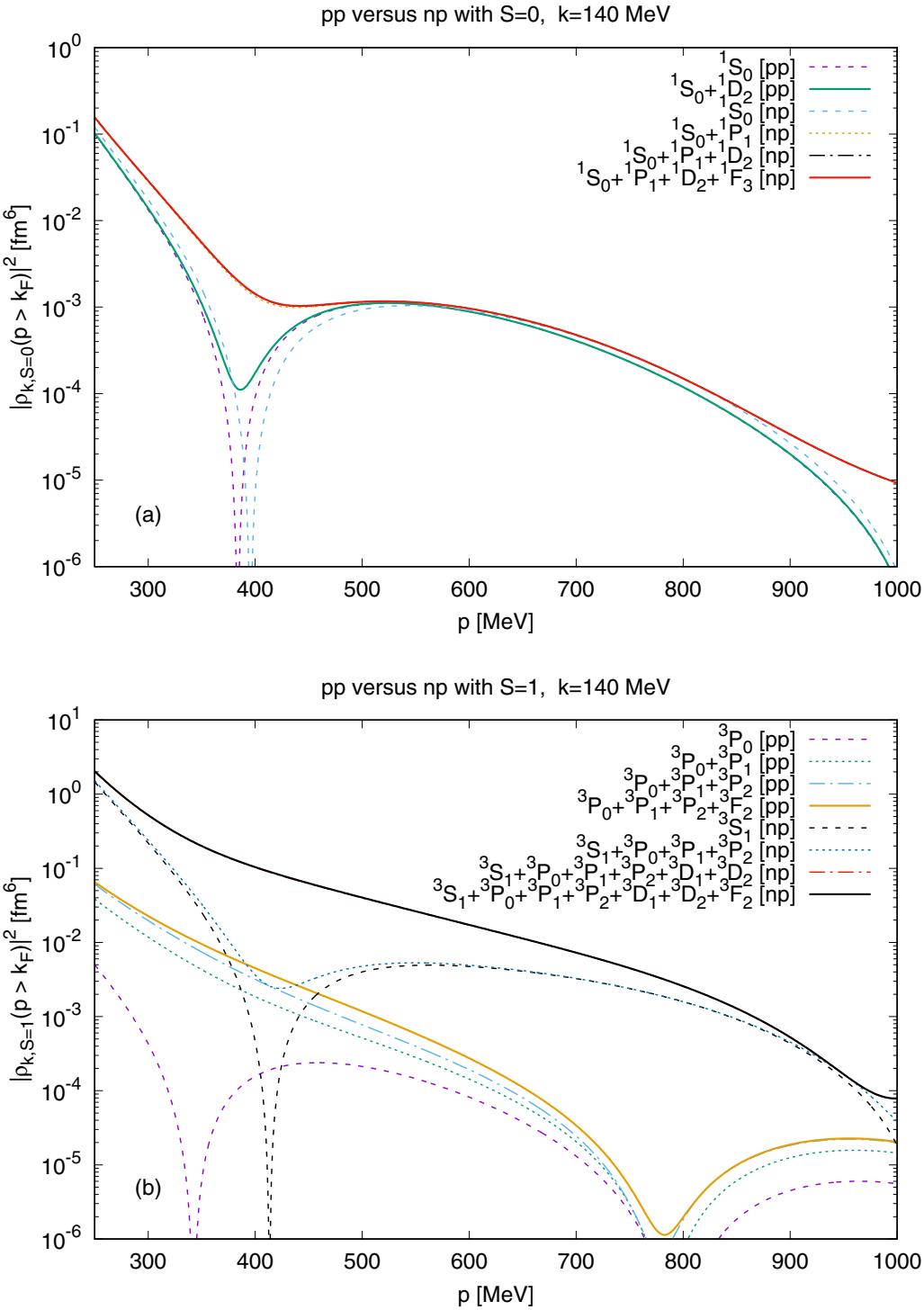

FIG. 8. Comparison of NN high-momentum distributions for np and pp pairs with different total spins, $S = 0,1$. In panel (a) we show the singlet ($S = 0$) high-momentum distribution, while in panel (b) we show the triplet ($S = 1$) case. The contributions of different partial waves are accumulatively added in each spin channel. The calculations have been performed for relative momentum of the nucleon pair $k = 140$ MeV.

where the SS term is the contribution of the $^3S_1$ wave to the high-momentum distribution of the $^3S_1$ wave (diagonal term), while the SD term is the contribution of the $^3D_1$ wave to the high-momentum distribution of the $^3S_1$ partial wave (mixing term). The DS and DD terms have an analogous meaning for the $^3D_1$ high-momentum distribution. Note that, although the δ-shell strengths are symmetric $(\lambda_i)_{\rm SD} = (\lambda_i)_{\rm DS}$, the SD and DS terms of Eqs. (40) and (41) are not equal. Now taking the module squared of Eqs. (40) and (41), three contributions come out for each partial

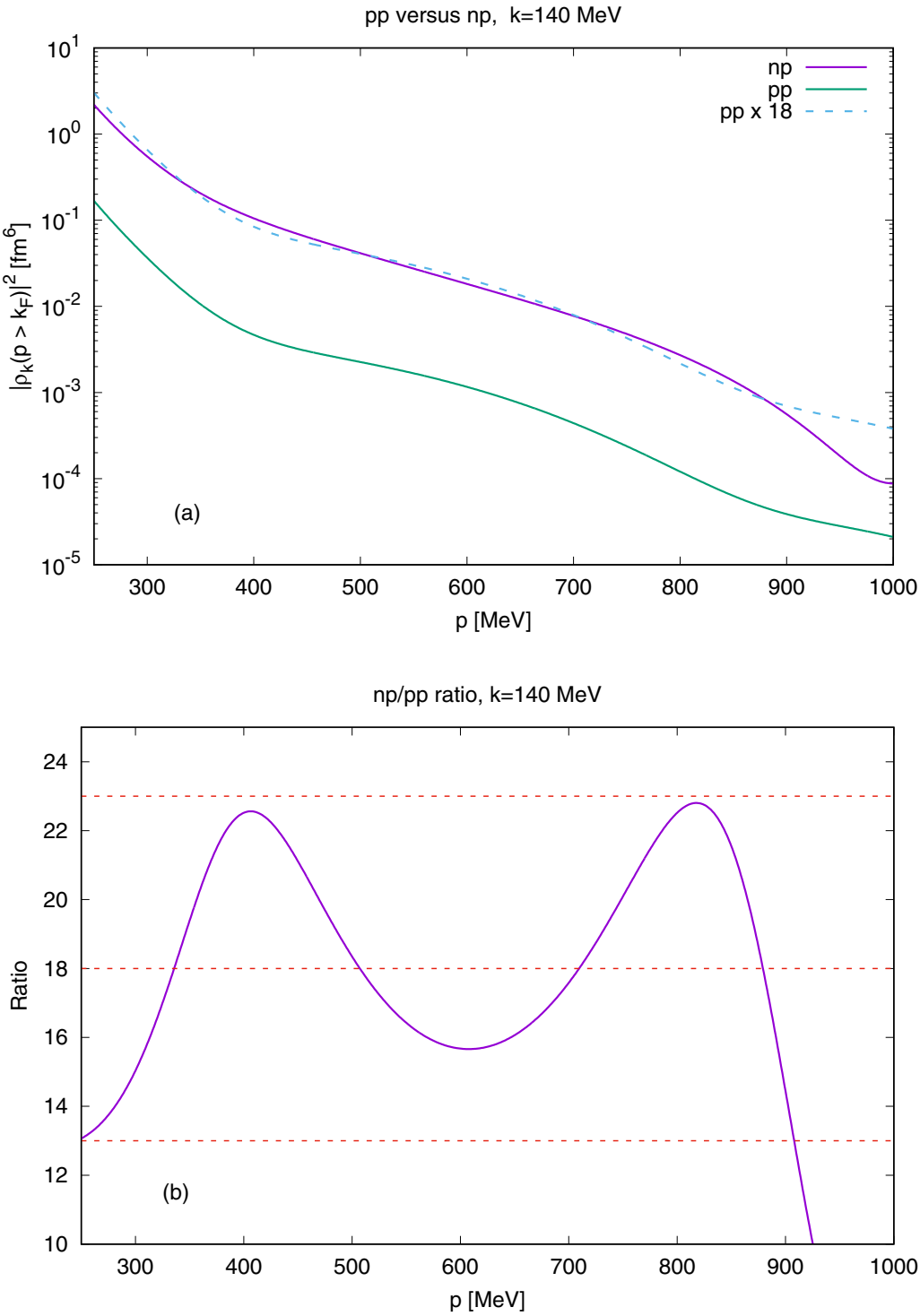

FIG. 9. (a) Comparison of total NN high-momentum distributions for np and pp pairs regardless of the total spin S. It is also displayed the curve corresponding to pp high-momentum components multiplied by the factor 18, as measured in Ref. [32]. (b) Ratio of the np over pp high-momentum distribution. The central value and extremal given by 18 ± 5, as measured in Ref. [32], are also displayed as horizontal dotted lines. The calculations have been performed for relative momentum of the nucleon pair $k = 140$ MeV.

wave

$$\left|\phi_{k,^3S_1}(p > k_F)\right|^2 = |\mathrm{SS} + \mathrm{SD}|^2 = |\mathrm{SS}|^2 + |\mathrm{SD}|^2 + 2\,\mathrm{Re}[\mathrm{SS}^* \times \mathrm{SD}], \quad (42)$$

and a similar expression for the $^3D_1$ case. These three separated contributions are plotted in Fig. 7. What can be observed in this figure is that the mixing terms (SD and DS) are generally the most important pieces contributing to the high-momentum distribution of the pair in this coupled channel. In fact, in the

$^3S_1$ wave the SD piece is dominant in the range below 400 MeV, while in the $^3D_1$ wave the DS-piece dominates in almost the full range of high momenta. From these results we conclude that the largest contribution to the high-momentum distribution tail of a nucleon pair in the deuteron channel comes from the mixing produced by the nondiagonal part of the NN interaction mixing the S and D waves, that is, by the tensor force again. If we set to zero this mixing (by setting SD = DS = 0), this large tail is considerably reduced in magnitude, because only the SS and DD terms survive, as can be seen in Fig. 7.

Notice that the interferences SS–SD and DS–DD can be negative for some ranges in the p variable. In fact, they are for sure at the nodes of the total (solid red line) curve, because the other contributions are always positive by construction. To represent all the components in the same logarithmic scale, we have plotted the absolute value of the interferences.

F. *pp* versus *np* high-momentum distributions

In Fig. 8 we compare the high-momentum distributions ($p > k_F$) for np and pp correlated pairs coupled to a definite spin, $S = 0,1$. The initial relative momentum of the back-to-back pair is $k = 140$ MeV. These distributions have been obtained by integrating $|\Phi^{\rm BG}_{\mathbf{k},SM_s}(\mathbf{p})|^2$ over the angles of the initial and final momenta, $\hat{\mathbf{k}}$ and $\hat{\mathbf{p}}$, and summing over all the M_s spin projections for a given spin S,

$$|\rho_{k,S}(p)|^2 \equiv \sum_{M_s}\int d\Omega_{\hat{\mathbf{k}}}\int d\Omega_{\hat{\mathbf{p}}}\left|\Phi^{\rm BG}_{\mathbf{k},SM_s}(\mathbf{p})\right|^2 = \sum_{L,J}(2J+1)|\phi_{k,LSJ}(p)|^2. \quad (43)$$

This is proportional to the probability density for a correlated pair with initial relative momentum k in any direction, and total spin S with any projection M_s, to be found with high relative momentum $p > k_F$ in any direction as well. Note that it is given as the sum of the squared of the radial wave functions for all the partial waves, multiplied by its multiplicity $(2J+1)$.

It can be observed from Fig. 8 that the high-momentum distribution for an np pair is larger than for the pp case, regardless of the spin. This is generally due to the fact that for np pairs more partial waves contribute than for a pp pair with a given total spin. For a pp pair with spin $S = 0$ only partial waves with even L contribute, due to the global antisymmetry of the wave function for two identical fermions. Conversely, for a pp pair with spin $S = 1$, only partial waves with an odd value of L contribute. However, for np pairs all partial waves contribute because of the presence of two possible isospin combinations, $T = 0,1$.

In general, pp high-momentum distributions for $S = 0$ and for $S = 1$ are comparable in magnitude (except for the position of their minima). However, this is not the case for the np high-momentum distributions: the triplet ($S = 1$) distribution is one order of magnitude larger than the singlet ($S = 0$). This effect is mainly due to the tensor force, which is absent in the singlet channel and is only present in the triplet one. The most important contributions to the high-momentum distribution for an np pair with $S = 1$ [Fig. 8(b)] are the coupled $^3S_1$–$^3D_1$ partial waves. For a pp pair in the triplet channel only partial waves with odd L are allowed, and this excludes the $^3S_1$–$^3D_1$ contribution. There is, of course, the presence of the coupled $^3P_2$–$^3F_2$ channel, but its contribution to the high-momentum components is generally small.

These features encountered here for the two-nucleon high-momentum distributions are in agreement with those found in other studies of the high-momentum distributions of finite nuclei and nuclear matter [15,32,69–71] for a wide variety of nuclei. These results provide support for the approach we have initiated in this work to solve the BG equation with a coarse-grained potential.

In Fig. 9 we show the comparison between the high-momentum distributions of np and pp correlated pairs, for initial momentum $k = 140$, regardless of the total spin of the pair. This amounts to carrying out an additional sum in Eq. (43) over the two possible total spins, $S = 0,1$. From the figure it appears that the high-momentum components for correlated np pairs are much larger than for pp pairs. This is a well-known feature of SRC with wide experimental support. In fact in the recent JLab experiment of Ref. [32], a factor 18 ± 5 was reported between the np and pp high-momentum correlated pairs in the

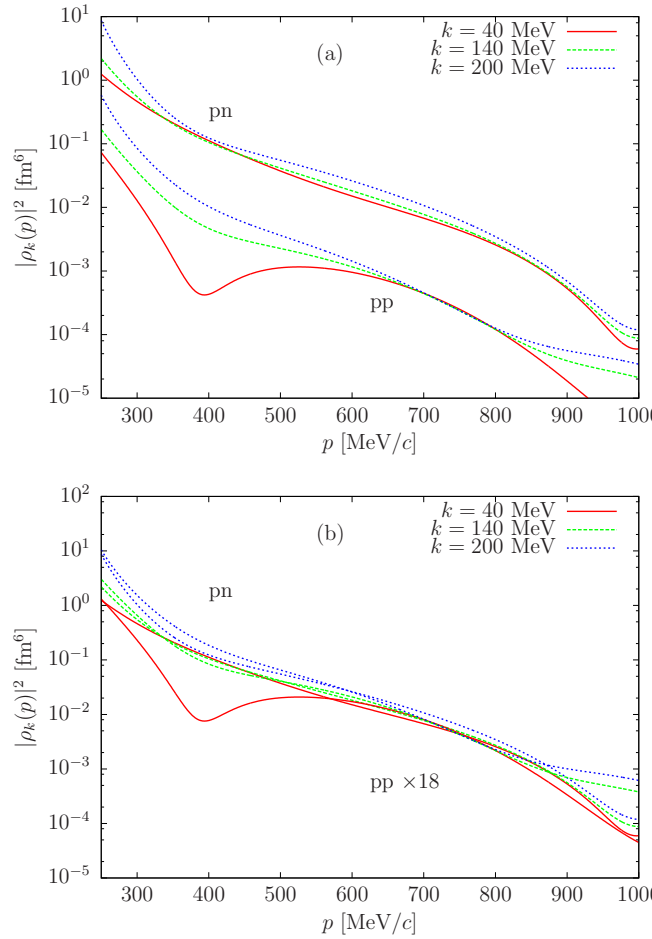

FIG. 10. (a) Comparison of high-momentum distributions for np and pp pairs for three different values of the initial momentum k. (b) The same as the panel (a) but with the pp distribution multiplied by a factor 18.

^{12}C ground state. This factor is in respectable accord with the results in Fig. 9. In fact when we multiply the pp distribution by a factor 18, it is very similar to the np one. Moreover, if we plot the ratio np/pp (lower panel of Fig. 9), then we find it to be inside the same interval 18 ± 5 reported in Ref. [32].

Finally, in Fig. 10 we make the same np/pp comparison for three different values of the initial momentum $k = 40, 140$, and 200 MeV. While the high-momentum distribution is found to be dependent on k, the factor 18 between both distribution is quite stable for the three values of k considered. Therefore, although it is out of the scope of the present work, one expects that the same factor be approximately valid also for the total momentum distribution.

V. CONCLUSIONS

In this work we have obtained the high-momentum distributions for a correlated nucleon pair in nuclear matter by solving the Bethe–Goldstone equation in coordinates representation for the original coarse-grained NN potential used *directly* to generate the Granada-2013 database, a 3σ self-consistent selection of 6173-NN-scattering data from the about 8000 collected since 1950 until 2013 at about pion production threshold, $T_{\rm LAB} = 350$ MeV with a reduced $\chi^2/\nu \sim 1.04$ [51–53]. This calculation has been done without introducing a further smooth potential, as it has been usually the case in the past with the so-called high-quality potentials descending from the benchmarking Nijmegen analysis 25 years ago. This way we avoid a source of systematic bias.

The method is based on solving the integral Bethe–Goldstone equation for a nucleon pair with total momentum of the pair $\mathbf{P} = \mathbf{0}$ and relative momentum $\mathbf{k}$. The application of the method for a coarse-grained potential consisting on δ shells located at some equally spaced concentration radii below 3 fm is very simple. It only consists on inverting a 5×5 linear system of equations for the uncoupled partial waves and a 10×10 matrix for the partial waves coupled by the tensor force.

The effects of the mixing due to the tensor force in some partial waves are very important, especially for the $^3S_1$–$^3D_1$ channel, which is only present in the neutron–proton high-momentum distribution and makes it to be much larger than its proton–proton counterpart. More specifically, we find that the probability of finding a high-momentum correlated np pair is about 18 times that of a pp pair, as a result of the strong tensor force, thus confirming in an independent way previous results and measurements. This important finding is coincident with those of previous studies carried out for different nuclei [15,32,69–71].

Future extensions of this work include the treatment of the center of mass of the nucleon pair, which will allow us to widen our calculations for $\mathbf{P} \neq \mathbf{0}$. While it has traditionally been handled by the averaging method of Brueckner, we expect it to be manageable by means of perturbative methods. A more ambitious goal requires considering the mixing among all partial waves induced by the Pauli-blocking operator. For the coarse-grained potential considered in this work, this can be accomplished in a partial expansion terminating at a maximum total angular momentum $J_{\rm max}$. This requires inverting, at most, a $5J_{\rm max}$- or $10J_{\rm max}$-dimensional matrices for uncoupled and coupled channels, respectively.

We also plan to try perturbation theory right from the beginning by adequately renormalizing the wave function in the first iteration [note that Eq. (19) can be, in principle, iteratively solved]. This was found to be possible for the $^1S_0$ case in Ref. [55]. If it were found the same for the other partial waves calculated in this work, the SRC could be consistently incorporated in our super-scaling approach with meson-exchange currents formalism [72,73] to calculate multinucleon emission in neutrino and electron scattering.

ACKNOWLEDGMENTS

This work has been partially supported by Spanish Ministerio de Economia y Competitividad and ERDF (European Regional Development Fund) under contract FIS2014- 59386-P, by Junta de Andalucia Grant No. FQM-225, and by Lawrence Livermore National Laboratory under Contract No. DEAC52-07NA27344, U.S. Department of Energy, Office of Science, Office of Nuclear Physics under Award No. desc0008511 (NUCLEI SciDAC Collaboration). One of us, IRS, acknowledges support from a Juan de la Cierva-incorporacion fellowship from MINECO (Spain).

[1] R. Jastrow, Phys. Rev. **79**, 389 (1950).
[2] R. Jastrow, Phys. Rev. **81**, 165 (1951).
[3] H. A. Bethe and J. Goldstone, Proc. Roy. Soc. (London) **A238**, 551 (1957).
[4] L. Gomes, J. D. Walecka, and V. F. Weisskopf, Ann. Phys. **3**, 241 (1958).
[5] F. Coester and H. Kümmel, Nucl. Phys. **17**, 477 (1960).
[6] H. Muther and A. Polls, Prog. Part. Nucl. Phys. **45**, 243 (2000).
[7] H. Feldmeier, W. Horiuchi, T. Neff, and Y. Suzuki, Phys. Rev. C **84**, 054003 (2011).
[8] M. Alvioli, C. Ciofi degli Atti, L. P. Kaptari, C. B. Mezzetti, H. Morita, and S. Scopetta, Phys. Rev. C **85**, 021001 (2012).
[9] M. Alvioli, C. Ciofi Degli Atti, L. P. Kaptari, C. B. Mezzetti, and H. Morita, Int. J. Mod. Phys. E **22**, 1330021 (2013).
[10] A. Ramos, A. Polls, and W. H. Dickhoff, Nucl. Phys. A **503**, 1 (1989).
[11] Y. Dewulf, W. H. Dickhoff, D. Van Neck, E. R. Stoddard, and M. Waroquier, Phys. Rev. Lett. **90**, 152501 (2003).
[12] B. E. Vonderfecht, W. H. Dickhoff, A. Polls, and A. Ramos, Phys. Rev. C **44**, R1265(R) (1991).
[13] S. Fantoni and V. R. Pandharipande, Nucl. Phys. A **427**, 473 (1984).
[14] H. Muther, A. Polls, and W. H. Dickhoff, Phys. Rev. C **51**, 3040 (1995).
[15] R. B. Wiringa, R. Schiavilla, S. C. Pieper, and J. Carlson, Phys. Rev. C **89**, 024305 (2014).
[16] O. Benhar, C. Ciofi Degli Atti, S. Liuti, and G. Salmè, Phys. Lett. B **177**, 135 (1986).
[17] J. W. Van Orden, W. Truex, and M. K. Banerjee, Phys. Rev. C **21**, 2628 (1980).

[18] L. Frankfurt, M. Sargsian, and M. Strikman, Int. J. Mod. Phys. A **23**, 2991 (2008).
[19] O. Hen, B.-A. Li, W.-J. Guo, L. B. Weinstein, and E. Piasetzky, Phys. Rev. C **91**, 025803 (2015).
[20] C. Xu and B.-A. Li, arXiv:1104.2075 [nucl-th].
[21] D. Ding, A. Rios, H. Dussan, W. H. Dickhoff, S. J. Witte, A. Carbone, and A. Polls, Phys. Rev. C **94**, 025802 (2016) [Addendum: **94**, 029901 (2016)].
[22] G. Röpke, Phys. Rev. C **92**, 054001 (2015).
[23] A. Mukherjee, Phys. Rev. C **79**, 045811 (2009).
[24] W. Broniowski and M. Rybczynski, Phys. Rev. C **81**, 064909 (2010).
[25] F. Simkovic, A. Faessler, H. Muther, V. Rodin, and M. Stauf, Phys. Rev. C **79**, 055501 (2009).
[26] M. Kortelainen and J. Suhonen, Phys. Rev. C **76**, 024315 (2007).
[27] L. L. Frankfurt, M. I. Strikman, D. B. Day, and M. Sargsyan, Phys. Rev. C **48**, 2451 (1993).
[28] L. B. Weinstein, E. Piasetzky, D. W. Higinbotham, J. Gomez, O. Hen, and R. Shneor, Phys. Rev. Lett. **106**, 052301 (2011).
[29] C. Giusti, H. Muther, F. D. Pacati, and M. Stauf, Phys. Rev. C **60**, 054608 (1999).
[30] J. Ryckebusch, M. Vanderhaeghen, K. Heyde, and M. Waroquier, Phys. Lett. B **350**, 1 (1995).
[31] C. Colle, O. Hen, W. Cosyn, I. Korover, E. Piasetzky, J. Ryckebusch, and L. B. Weinstein, Phys. Rev. C **92**, 024604 (2015).
[32] R. Subedi *et al.*, Science **320**, 1476 (2008).
[33] K. S. Egiyan *et al.* (CLAS Collaboration), Phys. Rev. Lett. **96**, 082501 (2006).
[34] I. Korover *et al.* (Jefferson Lab Hall A Collaboration), Phys. Rev. Lett. **113**, 022501 (2014).
[35] R. Shneor *et al.* (Jefferson Lab Hall A Collaboration), Phys. Rev. Lett. **99**, 072501 (2007).
[36] N. Fomin *et al.*, Phys. Rev. Lett. **108**, 092502 (2012).
[37] O. Hen *et al.*, Science **346**, 614 (2014).
[38] A. Tang, J. W. Watson, J. Aclander, J. Alster, G. Asryan, Y. Averichev, D. Barton, V. Baturin, N. Bukhtoyarova, A. Carroll, S. Gushue, S. Heppelmann, A. Leksanov, Y. Makdisi, A. Malki, E. Minina, I. Navon, H. Nicholson, A. Ogawa, Y. Panebratsev, E. Piasetzky, A. Schetkovsky, S. Shimanskiy, and D. Zhalov, Phys. Rev. Lett. **90**, 042301 (2003).
[39] R. Starink *et al.*, Phys. Lett. B **474**, 33 (2000).
[40] W. U. Boeglin *et al.* (Hall A Collaboration), Phys. Rev. Lett. **107**, 262501 (2011).
[41] J. J. van Leeuwe *et al.*, Phys. Rev. Lett. **80**, 2543 (1998).
[42] M. Oertel, M. Hempel, T. Klähn, and S. Typel, Rev. Mod. Phys. **89**, 015007 (2017).
[43] S. Stevens, J. Ryckebusch, W. Cosyn, and A. Waets, arXiv:1707.05542 [nucl-th].
[44] V. G. J. Stoks, R. A. M. Klomp, M. C. M. Rentmeester, and J. J. de Swart, Phys. Rev. C **48**, 792 (1993).
[45] V. Stoks and J. J. de Swart, Phys. Rev. C **47**, 761 (1993).
[46] V. G. J. Stoks and J. J. de Swart, Phys. Rev. C **52**, 1698 (1995).
[47] V. G. J. Stoks, R. A. M. Klomp, C. P. F. Terheggen, and J. J. de Swart, Phys. Rev. C **49**, 2950 (1994).
[48] R. B. Wiringa, V. G. J. Stoks, and R. Schiavilla, Phys. Rev. C **51**, 38 (1995).
[49] R. Machleidt, Phys. Rev. C **63**, 024001 (2001).
[50] F. Gross and A. Stadler, Phys. Rev. C **78**, 014005 (2008).
[51] R. Navarro Pérez, J. E. Amaro, and E. Ruiz Arriola, Phys. Rev. C **88**, 024002 (2013); **88**, 069902(E) (2013).
[52] R. Navarro Pérez, J. E. Amaro, and E. Ruiz Arriola, Phys. Rev. C **88**, 064002 (2013); **91**, 029901(E) (2015).
[53] J. E. Amaro, R. Navarro Pérez, and E. Ruiz Arriola, 2013 Granada Database [http://www.ugr.es/ amaro/nndatabase/].
[54] R. Navarro Pérez, J. E. Amaro, and E. Ruiz Arriola, J. Phys. G **43**, 114001 (2016).
[55] I. R. Simo, R. N. Perez, J. E. Amaro, and E. Ruiz Arriola, Phys. Rev. C **95**, 054003 (2017).
[56] P. Fernandez-Soler and E. Ruiz Arriola, Phys. Rev. C **96**, 014004 (2017).
[57] I. Ruiz Simo, J. E. Amaro, E. Ruiz Arriola, and R. Navarro Pérez, arXiv:1705.06522 [nucl-th].
[58] E. Werner, Nucl. Phys. **10**, 688 (1959).
[59] K. A. Brueckner and J. L. Gammel, Phys. Rev. **109**, 1023 (1958).
[60] K. Suzuki, R. Okamoto, M. Kohno, and S. Nagata, Nucl. Phys. A **665**, 92 (2000).
[61] F. Sammarruca, X. Meng, and E. J. Stephenson, Phys. Rev. C **62**, 014614 (2000).
[62] L. White and F. Sammarruca, Phys. Rev. C **88**, 054619 (2013).
[63] L. White and F. Sammarruca, Phys. Rev. C **90**, 044607 (2014).
[64] R. D. Viollier and J. D. Walecka, Acta Phys. Polon. B **8**, 25 (1977).
[65] D. Levin, Jour. Comput. Appl. Math. **67**, 95 (1996).
[66] D. Levin, Jour. Comput. Appl. Math. **78**, 131 (1997).
[67] R. N. Perez, J. E. Amaro, and E. Ruiz Arriola, Phys. Rev. C **95**, 064001 (2017).
[68] M. Alvioli, C. Ciofi degli Atti, and H. Morita, Phys. Rev. C **94**, 044309 (2016).
[69] R. Schiavilla, R. B. Wiringa, S. C. Pieper, and J. Carlson, Phys. Rev. Lett. **98**, 132501 (2007).
[70] M. M. Sargsian, T. V. Abrahamyan, M. I. Strikman, and L. L. Frankfurt, Phys. Rev. C **71**, 044615 (2005).
[71] J. Ryckebusch, W. Cosyn, and M. Vanhalst, J. Phys. G **42**, 055104 (2015).
[72] G. D. Megias, J. E. Amaro, M. B. Barbaro, J. A. Caballero, T. W. Donnelly, and I. R. Simo, Phys. Rev. D **94**, 093004 (2016).
[73] I. Ruiz Simo, J. E. Amaro, M. B. Barbaro, A. De Pace, J. A. Caballero, and T. W. Donnelly, J. Phys. G **44**, 065105 (2017).